

DATA ASSIMILATION WITH HIGHER ORDER FINITE ELEMENT INTERPOLANTS

MICHAEL S. JOLLY AND ALI PAKZAD

ABSTRACT. The efficacy of a nudging data assimilation algorithm using higher order finite element interpolating operators is studied. Numerical experiments are presented for the 2D Navier-Stokes equations in two cases: shear flow in an annulus and a forced flow in a disk with an off-center cavity. In both cases second order interpolation of coarse-grain data is shown to outperform first order interpolation. Convergence of the nudged solution to that of a direct numerical reference solution is proved. The analysis points to a trade-off in the estimates for higher order interpolating operators.

1. INTRODUCTION

In rough terms, data assimilation refers to a class of methodologies which observational data is combined with a model in order to improve the accuracy in forecasts. These techniques have been used for a long time in weather modeling, climate science, and hydrological and environmental forecasting [49]. There are a variety of data assimilation techniques, whereby actual measured quantities over time are incorporated in system models. Best known perhaps is the Kalman filter, which for discrete in time, linear systems give exact probabilistic predictions consistent with uncertainties in the both the data and the model. This Bayesian approach is adapted to nonlinear systems in extended Kalman filters, though they are no longer exact. Variational methods, 3DVar and 4DVar also track such uncertainties for discrete systems. More on these methods can be found in the books [2, 17, 47].

Continuous, deterministic data assimilation injects an interpolant of the data, assumed to be known for all time in some interval, directly into a differential equation. Charney, Halem and Jastrow proposed inserting low Fourier mode data into the advective term of the Navier-Stokes equations (NSE), [12, 33]. That approach can be interpreted through the result of Foias and Prodi [29] showing that there are a finite number of determining modes for the 2D NSE. Quantities such as volume elements and nodal values have also been shown to be determining [13, 15, 44]. While these quantities are more readily measured in practice, inserting them into the advective term is problematic. The technique of nudging avoids the need for derivatives by using this data in a linear

Date: August 10, 2021.

2010 *Mathematics Subject Classification.* Primary 35Q30, 76B75, 34D06; Secondary 35Q35, 35Q93.

Key words and phrases. Data assimilation, Navier-Stokes, Finite-elements.

The research of M. Jolly was supported in part by NSF grant DMS-1818754. The authors acknowledge the Lilly Endowment, Inc., through its support for the Indiana University Pervasive Technology Institute, which provided supercomputing resources used for this research <https://doi.org/10.5967/K8G44NGB>.

feedback term. For a model given by

$$(1.1) \quad \frac{d\mathbf{u}}{dt} = \mathbf{F}(\mathbf{u})$$

whose solution is known over a coarse grid of resolution H as $I_H \mathbf{u}(t)$, nudging is done through the auxiliary system

$$(1.2) \quad \frac{d\mathbf{v}}{dt} = \mathbf{F}(\mathbf{v}) - \mu I_H(\mathbf{v} - \mathbf{u}), \quad \mathbf{v}(0) = 0.$$

There is literature devoted to a form of this technique for synchronization of chaotic dynamical systems. See [3, 52] for a more complete history dating back to [36], and [51, 55] for comparisons with Kalman filtering.

For (1.1) given by the 2D NSE, Azouani, Olson and Titi showed that for large enough μ and small enough H , $\|\mathbf{v} - \mathbf{u}\| \rightarrow 0$ at an exponential rate [4]. Such analysis has since been completed for a variety of PDEs modeling physical phenomena [8, 21, 39–41, 50, 53, 56], in some instances, using data in only a subset of system variables [18, 20, 22–24] and more recently, over a subdomain of the physical spatial domain [9]. Though deterministic, the nudging approach has been studied with respect to error in the observed data [5, 39]. Computational experiments have demonstrated that nudging is effective using data that is much more coarse than the rigorous estimates require [1, 19, 31, 34], supported in some cases by analysis of certain numerical schemes [28, 48].

Nudging has also been studied for use with finite element method (FEM). Uniform in time error estimates in the semi-discrete case are made in [30]. Fully discrete FEM nudging schemes are shown to be well posed and stable in [45]. Both works analyze the error between the reference solution of the 2D NSE and the finite dimensional numerical scheme, and test the efficacy numerically in cases where the exact reference solution is specified over the square $[0, 1]^2$, and the corresponding body force added. A numerical test of 2D channel flow past a cylinder is also done in [45], in which case the reference solution is taken to be the result of a direct FEM numerical simulation over a fine mesh. Both works also focus on the case where interpolating operator satisfies

$$(1.3) \quad \|I_H \mathbf{u} - \mathbf{u}\|_{L^2} \leq c H \|\nabla \mathbf{u}\|_{L^2},$$

which is achieved by taking constant values over each triangle in a FEM discretization.

In this paper we present numerical evidence to show that higher order interpolation can achieve faster synchronization by nudging. This is suggested by the bound

$$(1.4) \quad \|\phi - I_H^k \phi\|_m \leq C_{k+1,m} H^{k+1-m} \|\phi\|_{k+1},$$

for k -degree polynomial over each triangle [10]. Two flows are tested: a shear flow in an annulus, and one with a body force in a disk with an off-center obstacle, both satisfying Dirichlet boundary conditions. For the shear flow we demonstrate that using a quadratic interpolating polynomial ($k = 2$), nudging can succeed when the data is too coarse for using a linear polynomial ($k = 1$). When the data is finer, both synchronize to within machine precision, but the quadratic polynomial does so in less than one-third the time. Similarly, in the body force case, for data with a certain resolution H , the speed-up is about a factor of 2 when a quadratic interpolating polynomial is

used. As we do not have exact reference solutions for these flows, the errors are in terms of the difference between the nudged solution and that of a direct numerical simulation (DNS) on a fine mesh, triangles of diameter $h \ll H$. Synchronization with the true solution of the NSE by nudging with higher order interpolation is analyzed in [6]. Here, we include a proof in the semi-discrete case of convergence of the nudged solution to the DNS solution for interpolating polynomials of any order. While this limited analysis is not sensitive enough to show an advantage in using higher degree interpolation, it does indicate a trade-off between the higher power in (1.4) and the price one pays to close the estimates with an inverse inequality (2.3). The computational results provide evidence that the higher power wins.

2. NOTATION

Let Ω be an open, bounded region in \mathbb{R}^2 with a Lipschitz continuous boundary. Define the velocity space \mathbf{X} as

$$\mathbf{X} := \mathbf{H}_0^1(\Omega) = \{\mathbf{u} \in \mathbf{H}^1(\Omega) : \mathbf{u} = 0 \text{ on } \partial\Omega\},$$

and the pressure space Q as follows

$$Q(\Omega) := L_0^2(\Omega) = \{q \in L^2(\Omega) : \int_{\Omega} q \, dx = 0\}.$$

The closed subspace of divergence free functions is given by

$$\mathbf{V} := \{\mathbf{u} \in \mathbf{X} : (\nabla \cdot \mathbf{u}, q) = 0, \forall q \in Q\}.$$

We denote the (explicitly skew symmetrized) trilinear form $b : \mathbf{X} \times \mathbf{X} \times \mathbf{X} \rightarrow \mathbb{R}$ as

$$b(\mathbf{u}, \mathbf{v}, \mathbf{w}) := \frac{1}{2}(\mathbf{u} \cdot \nabla \mathbf{v}, \mathbf{w}) - \frac{1}{2}(\mathbf{u} \cdot \nabla \mathbf{w}, \mathbf{v}),$$

which has the following property

$$b(\mathbf{u}, \mathbf{v}, \mathbf{w}) = -b(\mathbf{u}, \mathbf{w}, \mathbf{v}),$$

and therefore

$$b(\mathbf{u}, \mathbf{v}, \mathbf{v}) = 0, \quad \forall \mathbf{u}, \mathbf{v} \in \mathbf{X}.$$

To discretize the equations, consider a regular mesh $\Omega_h \in \Omega$ with maximum triangle diameter length h . Let two finite-dimensional spaces $\mathbf{X}^h \subset \mathbf{X}$ and $Q^h \subset Q$ be finite element velocity and pressure spaces corresponding to an admissible triangulation of Ω . We further assume that \mathbf{X}^h and Q^h satisfy the following discrete inf-sup condition (the condition for div-stability)

$$(2.1) \quad \inf_{q^h \in Q^h} \sup_{\mathbf{v}^h \in \mathbf{X}^h} \frac{(q^h, \nabla \cdot \mathbf{v}^h)}{\|\nabla \mathbf{v}^h\|_0 \|q^h\|_0} \geq \beta^h > 0,$$

where $\beta^h > 0$ uniformly in h as $h \rightarrow 0$.

In most finite element discretizations of the NSE and related systems, the divergence-free constraint $\nabla \cdot \mathbf{u}^h = 0$ is only weakly enforced. What holds instead of the pointwise constraint is that a

numerical solution \mathbf{u}^h in \mathbf{X}^h satisfies $\mathbf{u}^h \in \mathbf{V}^h$, where $\mathbf{V}^h \subset \mathbf{X}^h$ is constructed as

$$\mathbf{V}^h := \{\mathbf{v}^h \in \mathbf{X}^h : (q^h, \nabla \cdot \mathbf{v}^h) = 0, \forall q^h \in Q^h\}.$$

2.1. Triangular Finite Elements. Consider the most common finite element mesh; triangular. We first give here two examples of conforming finite element basis functions that are used in our computation, for more details see [10].

- (1) $P_1 : C^0$ -piecewise linear on triangles ($\dim P_1 = 3$). On each element the basis function is of the form

$$\phi(x, y) = c_0 + c_1x + c_2y,$$

and thus the values of ϕ are uniquely determined once ϕ is specified at the three vertices.

- (2) $P_2 : C^0$ -piecewise quadratic on triangles ($\dim P_2 = 6$). On each triangle, the basis functions are full quadratic polynomials

$$\phi(x, y) = c_0 + c_1x + c_2y + c_3x^2 + c_4y^2 + c_5xy,$$

and thus six nodes are needed per element to determine ϕ . The standard nodes are chosen to be the vertices and midpoints of the edges of the triangle.

One way to construct a velocity-pressure element spaces which satisfy (2.1) is by considering

$$\begin{aligned} \mathbf{X}^h &= \{\mathbf{v}^h \in \mathbf{H}_0^1(\Omega) : \mathbf{v}^h|_\Delta \in P_k(\Delta), \forall \Delta \text{ in the mesh}\}, \\ Q^h &= \{q^h \in L_0^2(\Omega) \cap C^0(\Omega) : q^h|_\Delta \in P_{k-1}(\Delta), \forall \Delta \text{ in the mesh}\}. \end{aligned}$$

The choice $k = 2$, known as the Taylor-Hood elements [54], is one commonly used choice of velocity-pressure finite element spaces which satisfy the discrete inf-sup condition. In fact for any $k \geq 2$ the above choice of velocity-pressure element spaces \mathbf{X}^h, Q^h satisfies (2.1) [32, 42, 46].

Throughout this manuscript, the $L^2(\Omega)$ and $H^1(\Omega)$ norms will be denoted by $\|\cdot\|_0$ and $\|\cdot\|_1$ respectively, and the $L^2(\Omega)$ inner product is given by (\cdot, \cdot) . For $k \geq 2$, the cell-wise definition of the norms in Sobolev spaces $H^k(\Omega)$ will be considered since in these cases finite element functions do not possess the regularity for the global norm to be well defined. Therefore for $k \geq 2$ without loss of generality we denote

$$\|\cdot\|_k = \sum_{\Delta \in \text{Mesh}} \|\cdot\|_{H^k(\Delta)}.$$

Let Ω_H denote a coarse finite element mesh which is refined by successively joining midpoints with line segments, ultimately producing the finest mesh Ω_h , so $h \ll H$. The spacing h corresponds to our Direct Numerical Simulation (DNS), whose solution, \mathbf{u}^h , plays the role of the reference solution, with which we seek to synchronize. The spacing H corresponds in practice to points where the true solution is observed and the data is collected. We process the observables by a k -degree interpolating polynomial $I_H^k : \mathbf{H}^{k+1}(\Omega) \rightarrow L^2(\Omega)$, satisfying the following approximation property:

$$(2.2) \quad \|\phi - I_H^k \phi\|_m \leq C_{k+1,m} H^{k+1-m} \|\phi\|_{k+1},$$

for every $\phi \in \mathbf{H}^{k+1}$, where $C_{k+1,m}$ is independent of ϕ and the mesh, see [10]. The case of linear interpolation, $k = 1$, was considered for finite element discretizations in [30, 45] and is consistent

with the original assumption in [4]. In this paper we study the relative efficacy of using higher order interpolants in nudging. Each mesh is made sufficiently regular to satisfy the inverse inequality

$$(2.3) \quad \|\phi^h\|_k \leq \tilde{C}_{k,m} h^{m-k} \|\phi^h\|_m,$$

for every $\phi^h \in \mathbf{X}^h$, where $\tilde{C}_{k,m}$ is a constant independent of ϕ^h and the mesh [10]. The inequalities (2.2), (2.3) point to the trade-off in estimating the efficacy of nudging with higher order interpolants. While the higher power in H is beneficial, the inverse relation with h works against us. Some analysis balancing these two effects is given in section 6.

3. EQUATIONS

We consider the incompressible Navier-Stokes equations (NSE) with Dirichlet boundary condition

$$(3.1) \quad \begin{aligned} \mathbf{u}_t + (\mathbf{u} \cdot \nabla) \mathbf{u} - \nu \Delta \mathbf{u} + \nabla p &= \mathbf{f}, \\ \nabla \cdot \mathbf{u} &= 0, \end{aligned}$$

in the physical domain $\Omega \subset \mathbb{R}^2$. Here \mathbf{u} is the velocity, $\mathbf{f} = \mathbf{f}(x, t)$ is the known body force, p is the pressure, and ν is the kinematic viscosity. Let I_H be an interpolation operator satisfying (2.2), then corresponding data assimilation algorithm is given by the system

$$(3.2) \quad \begin{aligned} \mathbf{v}_t + (\mathbf{v} \cdot \nabla) \mathbf{v} - \nu \Delta \mathbf{v} + \nabla q &= \mathbf{f} - \mu I_H(\mathbf{v} - \mathbf{u}), \\ \nabla \cdot \mathbf{v} &= 0, \end{aligned}$$

where the initial value of \mathbf{v}_0 is arbitrary.

We consider two flows, one with a body force \mathbf{f} , and one without. In the case of body force, let λ_1 be the smallest eigenvalue of the Stokes operator, our complexity parameter is the Grashof number

$$(3.3) \quad G = \frac{1}{\nu^2 \lambda_1} \|\mathbf{f}\|_0,$$

otherwise it is the Reynolds number given as $Re \sim 1/\nu$.

We use an IMEX (implicit-explicit) scheme as the temporal discretization to avoid the solution of a nonlinear problem at each time step. In short, in this scheme, at time $t = t_{n+1}$ the nonlinear term $\mathbf{v}_{n+1} \cdot \nabla \mathbf{v}_{n+1}$ is replaced by $\mathbf{v}_n \cdot \nabla \mathbf{v}_{n+1}$, where \mathbf{v}_n is obtained from already computed solution at time $t = t_n$. The spatial discretization is the finite element method and we discretize in space via the Taylor-Hood element pair, although it can be extended also to any LBB-stable pair easily.

Algorithm 3.1. Given body force $\mathbf{f} \in L^\infty((0, \infty), L^2(\Omega))$, initial condition $\mathbf{v}_0 \in \mathbf{V}_h$, reference solution \mathbf{u}_{n+1}^h , and $(\mathbf{v}_n^h, q_n^h) \in \mathbf{X}^h \times Q^h$, compute $(\mathbf{v}_{n+1}^h, q_{n+1}^h) \in \mathbf{X}^h \times Q^h$ satisfying

$$(3.4) \quad \begin{aligned} \left(\frac{\mathbf{v}_{n+1}^h - \mathbf{v}_n^h}{\Delta t}, \Theta^h \right) + b(\mathbf{v}_n^h, \mathbf{v}_{n+1}^h, \Theta^h) + \nu (\nabla \mathbf{v}_{n+1}^h, \nabla \Theta^h) - (q_{n+1}^h, \nabla \cdot \Theta^h) \\ = (\mathbf{f}_{n+1}, \Theta^h) - \mu (I_H(\mathbf{v}_{n+1}^h - \mathbf{u}_{n+1}^h), \Theta^h), \end{aligned}$$

$$(3.5) \quad (\nabla \cdot \mathbf{v}_{n+1}^h, r^h) = 0,$$

for all $(\Theta^h, r^h) \in \mathbf{X}^h \times Q^h$.

The approximating solution \mathbf{v}^h with an arbitrary initial condition is computed using Algorithm 3.1, while $I_H(\mathbf{u}_{n+1})$ represents our observations of the system at a coarse spatial resolution at the time step t_{n+1} . Note that at the time t_{n+1} we have already obtained the relevant data about the true solution, therefore $I_H(\mathbf{u}_{n+1})$ is interpreted to be the most recent data. The well-posedness of the above algorithm (3.1) with constant interpolation, $k = 0$, is studied in [45].

4. COMPUTATIONAL STUDY I; SHEAR FLOW

One of the classic problems in experimental fluid dynamics is shear flow, where the boundary condition is tangential. As in the experiment of G.I. Taylor and M.M.A. Couette, we consider a 2D slice of flow between rotating cylinders [27]. The domain Ω is an annulus

$$\Omega = \{(x, y) \in \mathbb{R}^2 : x^2 + y^2 \leq 1^2 \text{ and } x^2 + y^2 \geq (0.1)^2\}.$$

The flow is driven by the rotational force at the outer circle in an absence of body force $\mathbf{f} = 0$, with no-slip boundary conditions imposed on the inner circle. The Reynolds number is taken to be $Re = 600$. In all experiments, the algorithms are implemented by using public domain finite element software FreeFEM++ [35], and was run on the Carbonate supercomputer at Indiana University.

4.1. Spatial Discretization. In this study, we have three relatively coarse meshes for the data, and one fine mesh for the DNS. Our coarsest mesh, Mesh Level 1, is parameterized by 20 mesh points around the outer circle and 18 mesh points around the immersed circle, then extended to all of Ω as a Delaunay mesh [16]. Mesh Level 2 is generated by splitting each triangle in Mesh Level 1 into 4 sub-triangles. Each grid in Mesh Level 2 is then split into 4 sub-triangles to generate Mesh Level 4. To create the finest mesh, Mesh Level 8, all triangles in Mesh Level 4 are split into 4. Figure 1 shows the first two levels. More details about the grids can be found in Table 1. In what follows, h stands for the finest mesh (Mesh Level 8) and H represents a coarse spatial resolution where the observational data are collected.

Mesh's Type	# Vertices	# Triangles	Max size of mesh
Mesh Level 1	164	290	0.389
Mesh Level 2	618	1160	0.194
Mesh Level 4	2396	4640	0.097
Mesh Level 8	9432	18560	0.048

TABLE 1. Details on the spatial meshes

4.2. Reference Solution. Since we do not have access to a true solution for this problem, we use the DNS solution as our reference solution. We first resolve all scales down to Kolmogorov dissipation scales $h \leq Re^{-\frac{1}{2}}$, Mesh Level 8, and then compute the DNS solution \mathbf{u}_{n+1}^h using the first order scheme Algorithm 3.1 but without nudging ($\mu = 0$). The Taylor-Hood mixed finite

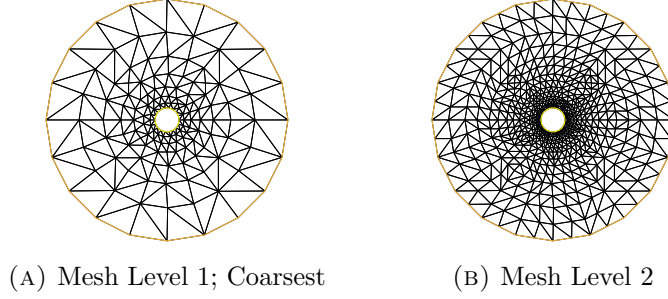


FIGURE 1. Mesh for flow between an annulus

elements are utilized for discretization in space on a Delaunay-Vornoi generated triangular mesh. The DNS is run from $t_0 = -5$ to a final time $T = 100$ with time step $\Delta t = 0.01$ starting from rest, i.e., $\mathbf{u}^h(t_0) = \mathbf{0}$.

The kinetic energy time series in Figure 2 shows the solution settling into regular oscillations. Without the true initial condition, then, one can expect at least a lag in another solution compared to the reference solution as shown on the right. More over, the L^2 norm of difference of two DNS solutions with two different initial conditions in Figure 2 indicates the sensitivity of the solution to the initial conditions as shown on the right.

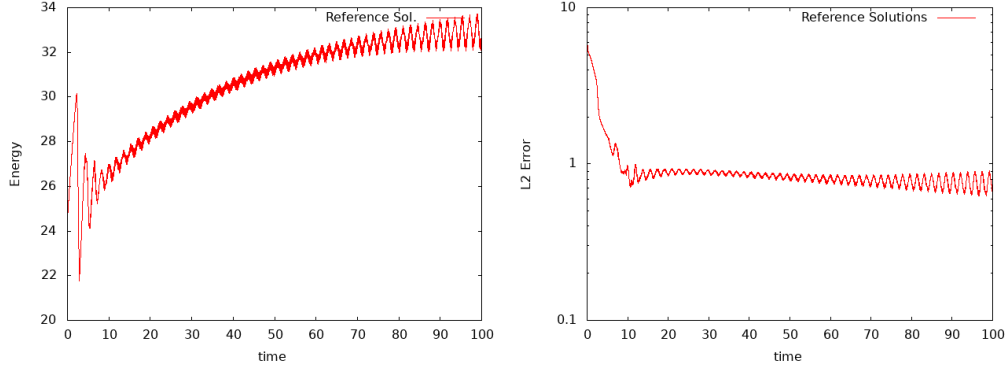


FIGURE 2. Left: kinetic energy of the reference solution \mathbf{u}^h . Right: $\|\mathbf{u}_1^h - \mathbf{u}_2^h\|_{L^2}$; \mathbf{u}_1^h and \mathbf{u}_2^h two reference solutions with different initial conditions

4.3. Nudged Solution. To compute the solution to (3.4), (3.5), we start from zero initial conditions, i.e., $\mathbf{v}_0^h = \mathbf{0}$, with $\mu = 100$ use the same spatial and temporal discretization parameters as for the DNS, and start nudging with the DNS solution. Interpolation I_H is carried out on the different refinement levels of spatial grids, while the equations (3.4), (3.5) are solved on the finest mesh.

To compare the effect of the higher order interpolation on the approximate solution, we consider linear and quadratic Lagrange interpolation. For simplicity, we first describe the idea locally on triangle with observational data available at six nodes; three at the vertices and three at midpoint of the edges of the triangle. For the interpolant, there are two options as shown in figure 3

- (1) Quadratic interpolation using the six nodes,
- (2) Refining the triangle to four sub-triangles. Linear interpolation on each of the four sub-triangles.

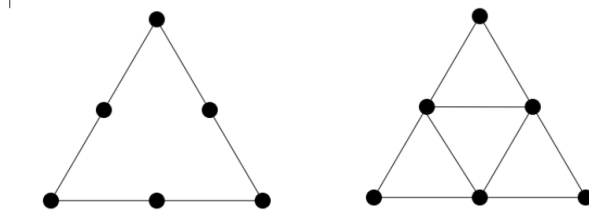


FIGURE 3. Quadratic interpolation using six nodes (left) versus linear interpolation on finer grid (right)

The time evolution of the L^2 and H^1 - norms for the difference in velocities of the reference and nudged solutions are shown in Figures 4, and 6. The simulations are made for linear and quadratic Lagrange interpolate with two data resolutions to determine the effect of the higher order interpolation of the error. In each case the interpolants use the same set of observed data. In short, in all mesh refinements, the synchronization is made at a better rate using quadratic interpolation in compare with the linear one. For data in Mesh Level 2, nudging with the quadratic interpolant achieves synchronization at an exponential rate, while the error using linear interpolation decays much slower, Figure 4. Figure 5 shows a zoom of the velocity vectors in the lower left quadrant of the domain, comparing the nudging approaches on Mesh level 2 with the result of DNS. The other quadrants are similar. Both methods synchronize to machine precision using data on Mesh Level 4, but the quadratic interpolant does so in roughly one-third the time, Figure 6. For data on Mesh Level 8, i.e., the irrelevant case of full knowledge of the reference solution, the errors are nearly the same, hence not shown here.

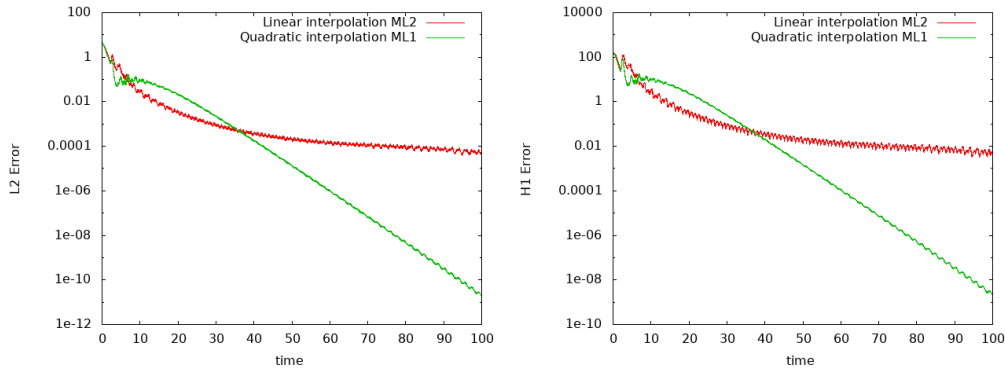


FIGURE 4. Data in Mesh Level 2. L^2 (left) H^1 (right) norm Error; Linear interpolation on Mesh Level 2 Vs. Quadratic interpolation on Mesh Level 1

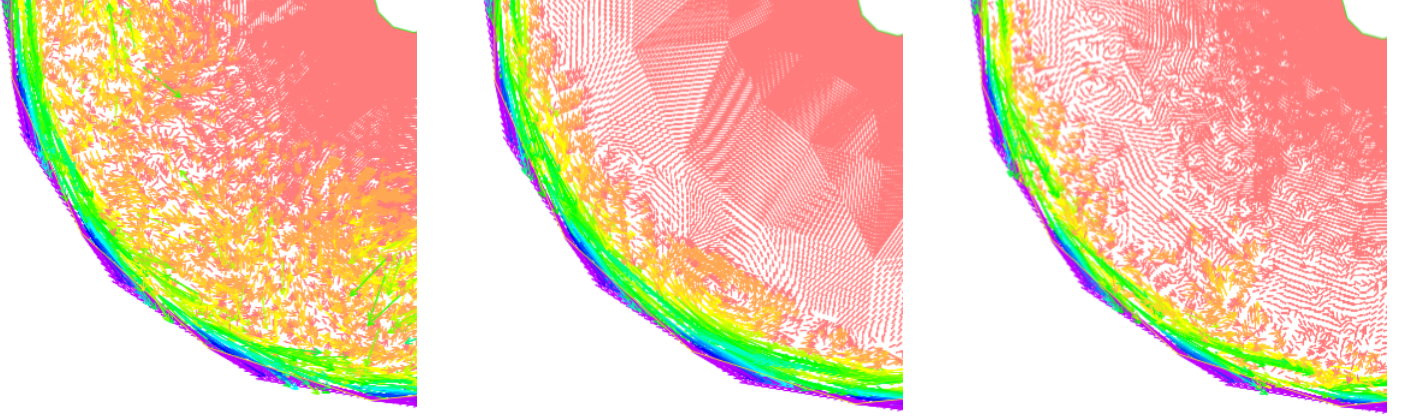


FIGURE 5. Velocity vector, shear flow at $t = 5$. Left: P1 interp. Mesh Level 2. Center: DNS (reference solution). Right: P2 interp. Mesh Level 1. Color indicates vector length: watermelon=0, purple=12

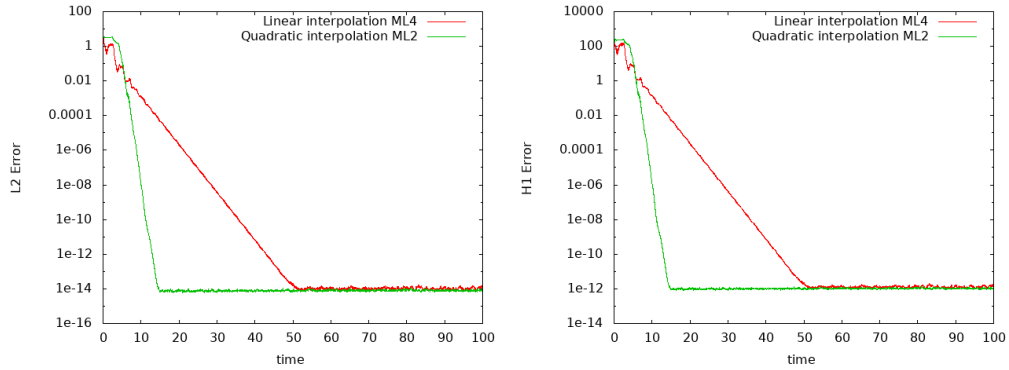


FIGURE 6. Data in Mesh level 4. L^2 (left) H^1 (right) norm Error; Linear interpolation on Mesh Level 4 Vs. Quadratic interpolation on Mesh Level 2

5. COMPUTATIONAL STUDY II ; BODY-FORCED CASE

In this study, we consider the two-dimensional flow between two offset circles. The domain is a disk with the omission of a smaller off-center disc inside given by

$$\Omega = \{(x, y) \in \mathbb{R}^2 : x^2 + y^2 \leq 1^2 \text{ and } (x - 0.5)^2 + y^2 \geq (0.1)^2\}.$$

No-slip, no-penetration boundary conditions are imposed on both circles, and the flow is driven by the counterclockwise rotational time-independent body force

$$\mathbf{f}(x, y) = (-4y(1 - x^2 - y^2), 4x(1 - x^2 - y^2))^\top.$$

As the flow rotates about the origin it interacts with the inner boundary generating complex flow structures including the formation of a Von Karman vortex street. This vortex street rotates and itself re-interacts with the immersed circle, creating more complex structures. All the simulations are run over the time interval $[0, 40]$ with a time-step size $\Delta t = 0.01$ and Reynolds number $Re = 600$, the same as done in [38]. We use the same mesh structures generated in the last section adapted to the new domain; one fine mesh for DNS, and three relatively coarse meshes levels for data.

5.1. Reference Solution. Again, since we do not have access to a true solution for this problem, we instead run a DNS and use the computed solution \mathbf{u}^h as the reference solution. The initial condition \mathbf{u}_0 , is generated by solving the steady Stokes problem with the same body forces $\mathbf{f}(x, y)$.

The fluctuations of the reference solution's kinetic energy in time, shown in Figure 7, is evidence of chaotic behavior. The sensitivity with respect to initial data is demonstrated by DNS with two different initial conditions, \mathbf{u}_{0_1} = generated by solving the steady state Stokes and $\mathbf{u}_{0_2} = \mathbf{0}$. The difference of the two solutions is plotted in Figure 7 right. This underscores the significance of a nudged solution synchronizing with the reference solution.

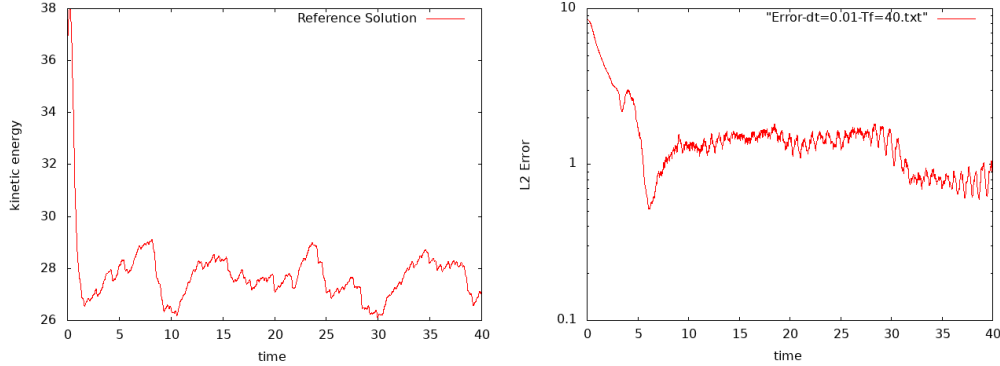


FIGURE 7. Left: Kinetic Energy of the reference solution, indicating chaos. Right: $\|\mathbf{u}_1^h - \mathbf{u}_2^h\|_{L^2}$, \mathbf{u}_1^h and \mathbf{u}_2^h two reference solutions with different initial conditions

5.2. Nudged Solution. As in the shear flow case we start from zero initial conditions $\mathbf{v}^h(0) = \mathbf{0}$, set $\mu = 10$, and use the same spatial and temporal discretization parameters as the DNS. While the nudging solution \mathbf{v}^h is computed on the fine mesh, Mesh Level 8, the interpolation I_H is either linear on the Mesh Level $2k$ or quadratic on the Mesh Level k , for $k = 1, 2$. As before, in both situations, we use the same amount of observational data (i.e. locally six nodes on each triangle). The L^2 and H^1 errors are plotted in Figures 9, and 10. In this case the data is too sparse on Mesh Level 2, for interpolation of either degree to synchronize to near machine precision. Figure 8 and 9 shows that although the quadratic interpolation has slightly better performance at the beginning,

nevertheless, both nudging captures the main features of the velocity field. Both interpolation methods synchronize using data on Mesh Level 4, with quadratic interpolation doing so in about one-half the time, Figure 10. As expected and like the shear flow case, errors are almost the same with complete knowledge of the flow, not shown here.

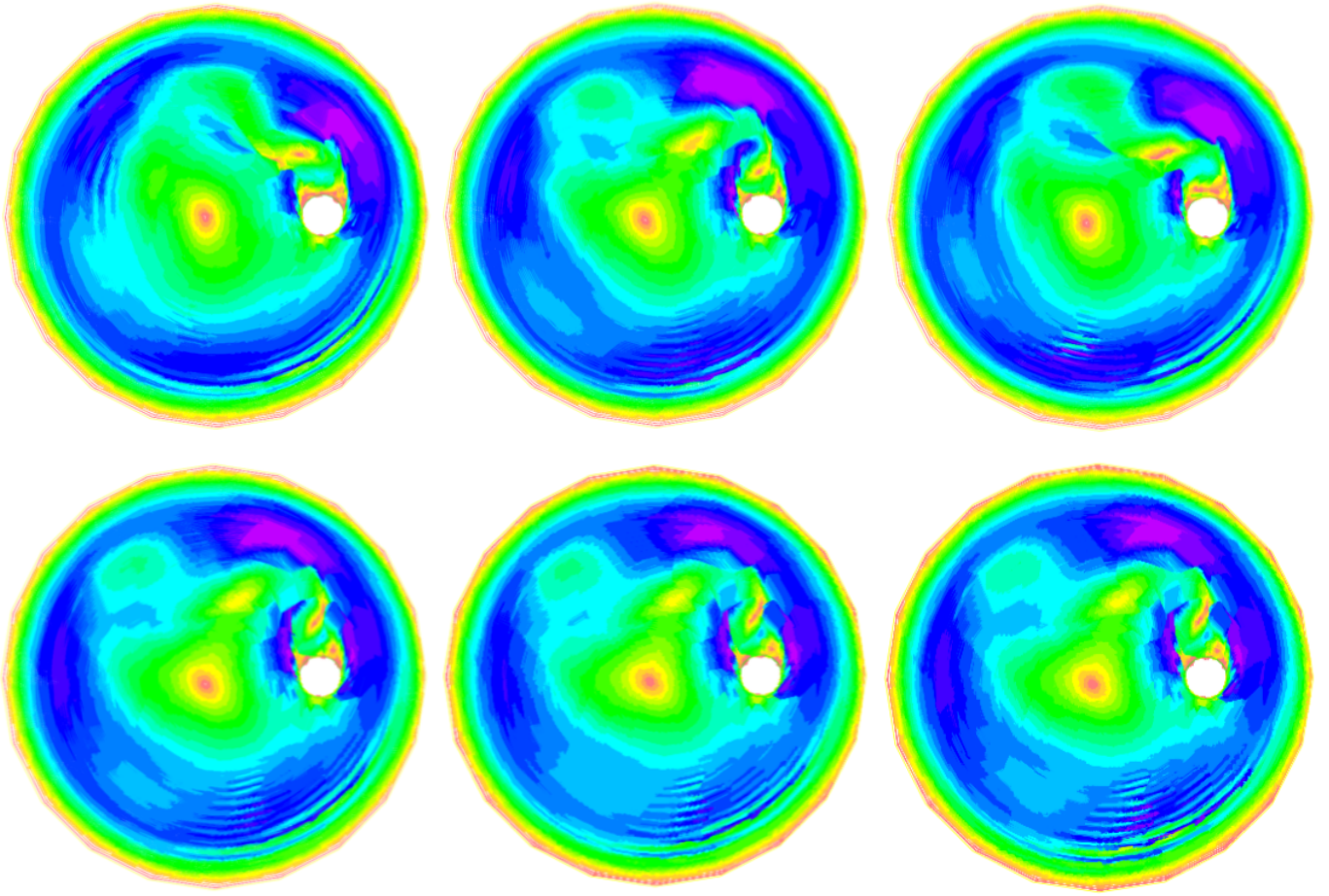


FIGURE 8. Velocity vector, body force flow. Top $t = 5$, bottom $t = 10$. Left: P1 interp. Mesh Level 2. Center: DNS (reference solution). Right: P2 interp. Mesh Level1. Color indicates vector length: orange = 0, blue ≈ 5 , purple ≈ 7

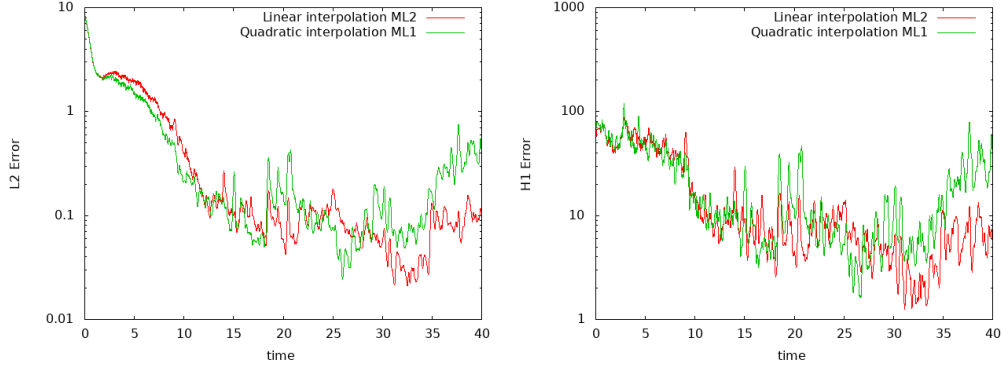


FIGURE 9. Data in Mesh Level 2. L^2 (left) H^1 (right) norm Error; Linear interpolation on Mesh Level 2 Vs. Quadratic interpolation on Mesh Level 1

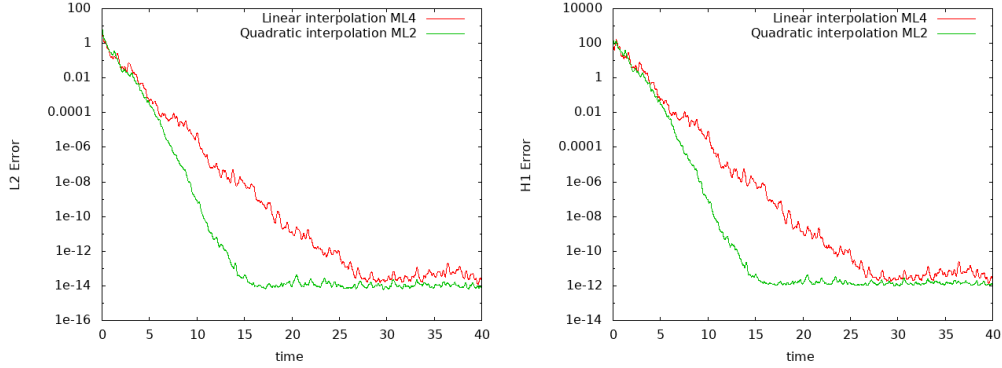


FIGURE 10. Data in Mesh Level 4. L^2 (left) H^1 (right) norm Error; Linear interpolation on Mesh Level 4 Vs. Quadratic interpolation on Mesh Level 2

6. CONTINUOUS TIME ANALYSIS

We have shown that quadratic interpolation can, in practice, outperform linear interpolation when used in nudging. A complete analysis to support this would be one stated in terms of bounds on $\|\mathbf{u} - \mathbf{v}^h\|_0$, as is done for constant and linear interpolation in [4]. To the best of our knowledge, these results have not yet been extended to higher order interpolation. While doing so, i.e., establishing that $\|\mathbf{u} - \mathbf{v}^h\|_0 \rightarrow 0$ as $t \rightarrow \infty$, when nudging with higher order interpolation may be straightforward, deriving an estimate that indicates an advantage of higher order interpolation is another matter. In this section, we sketch a proof of synchronization using higher order interpolation in the simpler case of a semi-discrete, continuous in time finite element approximation, and at the same time, illustrate the difficulty in demonstrating such an advantage over lower order interpolation.

To this end, we consider a reference solution satisfying the semi-discrete approximation

$$(6.1) \quad \begin{aligned} (\mathbf{u}_t^h, \Theta^h) + \nu (\nabla \mathbf{u}^h, \nabla \Theta^h) + b(\mathbf{u}^h, \mathbf{u}^h, \Theta^h) &= (f, \Theta^h), \\ (\mathbf{u}^h(\cdot, 0) - \mathbf{u}_0, \Theta^h) &= 0, \end{aligned}$$

for all $\Theta^h \in \mathbf{V}^h$, where, thanks to (2.1), the pressure has been eliminated by restricting the velocity to the space of discrete, divergence free functions \mathbf{V}^h . The continuous time nudging scheme is given by

$$(6.2) \quad \begin{aligned} (\mathbf{v}_t^h, \Theta^h) + \nu (\nabla \mathbf{v}^h, \nabla \Theta^h) + b(\mathbf{v}^h, \mathbf{v}^h, \Theta^h) &= (f, \Theta^h) - \mu (I_H^k(\mathbf{v}^h - \mathbf{u}^h), \Theta^h), \\ (\mathbf{v}^h(\cdot, 0) - \mathbf{v}_0, \Theta^h) &= 0, \end{aligned}$$

for any $\Theta^h \in \mathbf{V}^h$, where I_H^k is k^{th} order (degree) interpolating polynomial satisfying (2.2).

With the following decomposition of the nonlinear term

$$\begin{aligned} b(\mathbf{u}^h, \mathbf{u}^h, \Theta^h) - b(\mathbf{v}^h, \mathbf{v}^h, \Theta^h) &= b(\mathbf{u}^h, \mathbf{u}^h, \Theta^h) - b(\mathbf{v}^h, \mathbf{u}^h, \Theta^h) \\ &\quad + b(\mathbf{v}^h, \mathbf{u}^h, \Theta^h) - b(\mathbf{v}^h, \mathbf{v}^h, \Theta^h) \\ &= b(\mathbf{w}^h, \mathbf{u}^h, \Theta^h) + b(\mathbf{v}^h, \mathbf{w}^h, \Theta^h), \end{aligned}$$

the difference $\mathbf{w}^h = \mathbf{u}^h - \mathbf{v}^h \in \mathbf{V}^h$ satisfies

$$(\mathbf{w}_t^h, \Theta^h) + \nu (\nabla \mathbf{w}^h, \nabla \Theta^h) + b(\mathbf{w}^h, \mathbf{u}^h, \Theta^h) + b(\mathbf{v}^h, \mathbf{w}^h, \Theta^h) = -\mu (I_H \mathbf{w}^h, \Theta^h).$$

Setting $\Theta^h = \mathbf{w}^h$, the second nonlinear term vanishes because $b(\cdot, \cdot, \cdot)$ is explicitly skew-symmetrized. Thus

$$(6.3) \quad \frac{1}{2} \frac{d}{dt} \|\mathbf{w}^h\|_0^2 + \nu \|\mathbf{w}^h\|_1^2 = -\mu (I_H^k \mathbf{w}^h, \mathbf{w}^h) - b(\mathbf{w}^h, \mathbf{u}^h, \mathbf{w}^h).$$

Using Young's inequality, along with (2.2) and (2.3), we have

$$\begin{aligned} -\mu (I_H^k \mathbf{w}^h, \mathbf{w}^h) &= -\mu (I_H^k \mathbf{w}^h - \mathbf{w}^h + \mathbf{w}^h, \mathbf{w}^h) = \mu (\mathbf{w}^h - I_H^k \mathbf{w}^h, \mathbf{w}^h) - \mu \|\mathbf{w}^h\|_0^2 \\ &\leq \frac{\mu}{2} \|\mathbf{w}^h - I_H^k \mathbf{w}^h\|_0^2 + \frac{\mu}{2} \|\mathbf{w}^h\|_0^2 - \mu \|\mathbf{w}^h\|_0^2 \\ &\leq \frac{\mu}{2} C_{k+1,0}^2 H^{2k+2} \|\mathbf{w}^h\|_{k+1}^2 - \frac{\mu}{2} \|\mathbf{w}^h\|_0^2 \\ &\leq \frac{\mu}{2} C_{k+1,0}^2 H^{2k+2} \tilde{C}_{k+1,1}^2 h^{-2k} \|\mathbf{w}^h\|_1^2 - \frac{\mu}{2} \|\mathbf{w}^h\|_0^2 \\ &\leq \frac{\nu}{2} \|\mathbf{w}^h\|_1^2 - \frac{\mu}{2} \|\mathbf{w}^h\|_0^2, \end{aligned} \quad (6.4)$$

provided

$$(6.5) \quad \nu \geq \mu C_{k+1,0}^2 \tilde{C}_{k+1,1}^2 \left(\frac{H}{h} \right)^{2k} H^2.$$

The Hölder, Ladyzhenskaya ¹, Poincaré ², and Agmon ³ inequalities give us the following estimate on the nonlinear term in (6.3)

$$\begin{aligned}
 (6.6) \quad b(\mathbf{w}^h, \mathbf{u}^h, \mathbf{w}^h) &= \frac{1}{2}(\mathbf{w}^h \cdot \nabla \mathbf{u}^h, \mathbf{w}^h) - \frac{1}{2}(\mathbf{w}^h \cdot \nabla \mathbf{w}^h, \mathbf{u}^h) \\
 &\leq \frac{C}{2} \|\mathbf{u}^h\|_1 \|\mathbf{w}^h\|_{L^4}^2 + \frac{C}{2} \|\mathbf{u}^h\|_{L^\infty} \|\mathbf{w}^h\|_0 \|\mathbf{w}^h\|_1 \\
 &\leq \frac{C}{2} \|\mathbf{u}^h\|_1 \|\mathbf{w}^h\|_1 \|\mathbf{w}^h\|_0 + \frac{C}{2} \|\mathbf{u}^h\|_0^{\frac{1}{2}} \|\mathbf{u}^h\|_2^{\frac{1}{2}} \|\mathbf{w}^h\|_0 \|\mathbf{w}^h\|_1 \\
 &\leq \frac{\nu}{4} \|\mathbf{w}^h\|_1^2 + \frac{C}{4\nu} \|\mathbf{u}^h\|_1^2 \|\mathbf{w}^h\|_0^2 + \frac{\nu}{4} \|\mathbf{w}^h\|_1^2 + \frac{C}{4\nu} \|\mathbf{u}^h\|_0 \|\mathbf{u}^h\|_2 \|\mathbf{w}^h\|_0^2 \\
 &\leq \frac{\nu}{2} \|\mathbf{w}^h\|_1^2 + \frac{C}{4\nu} \left(\|\mathbf{u}^h\|_1^2 + \|\mathbf{u}^h\|_0 \|\mathbf{u}^h\|_2 \right) \|\mathbf{w}^h\|_0^2 \\
 &\leq \frac{\nu}{2} \|\mathbf{w}^h\|_1^2 + \frac{C}{2\nu\lambda_1} \|\mathbf{u}^h\|_2^2 \|\mathbf{w}^h\|_0^2.
 \end{aligned}$$

Substituting (6.4), (6.6) in (6.3), we have

$$(6.7) \quad \frac{d}{dt} \|\mathbf{w}^h\|_0^2 + \left(\mu - \frac{C}{\nu\lambda_1} \|\mathbf{u}^h\|_2^2 \right) \|\mathbf{w}^h\|_0^2 \leq 0.$$

We next use the following uniform Grönwall inequality proved in [43].

Lemma 6.1. *Let $\tau > 0$ be arbitrary and fixed. Suppose that $Y(t)$ is an absolutely continuous function which is locally integrable such that*

$$\frac{dY}{dt} + \alpha(t)Y \leq 0,$$

where

$$\limsup_{t \rightarrow \infty} \int_t^{t+\tau} \alpha(s) ds \geq \gamma > 0.$$

Then $Y(t) \rightarrow 0$ exponentially fast, as $t \rightarrow \infty$.

One can adapt an argument in [26] for the solution to the NSE, to show that there exists a time $t_0 > 0$ such that for all $t \geq t_0$ and $\tau > 0$

$$(6.8) \quad \int_t^{t+\tau} \|\mathbf{u}^h\|_2^2 ds \leq (c_0 e^{G^4} + \tau \nu \lambda_1) \nu \lambda_1 G^2,$$

where c_0 is a positive non-dimensional constant. Now with $\alpha(s) = \mu - \frac{C}{\nu\lambda_1} \|\mathbf{u}^h(s)\|_2^2$ in (6.7), take $\tau = \frac{1}{\nu\lambda}$, and assume

$$(6.9) \quad \mu \geq 2(c_0 e^{G^4} + 1) \nu \lambda_1 G^2,$$

¹ $\|\varphi\|_{L^4} \leq \|\varphi\|_1^{\frac{1}{2}} \|\nabla \varphi\|_1^{\frac{1}{2}}$.

² $\|\varphi\|_0 \leq \frac{1}{\sqrt{\lambda_1}} \|\varphi\|_1$, $\|\varphi\|_1 \leq \frac{1}{\sqrt{\lambda_1}} \|\varphi\|_2$.

³ $\|\varphi\|_{L^\infty} \leq \|\varphi\|_0^{\frac{1}{2}} \|\varphi\|_2^{\frac{1}{2}}$.

so that

$$\int_t^{t+(\nu\lambda)^{-1}} \left(\mu - \frac{C}{\nu\lambda_1} \|\mathbf{u}^h(s)\|_2^2 \right) ds \geq (c_0 e^{G^4} + 1) G^2 = \gamma > 0,$$

and by Lemma 6.1 it follows that $\|\mathbf{w}^h\|_0 \rightarrow 0$ at an exponential rate.

Remark 6.2. Using an alternative approach, we can avoid the exponential factor in G , at the cost of cancelling H^{-2} factor in (6.13). Taking $\Theta = \mathbf{u}^h$ in (6.1), one finds there exists $t_0 > 0$, such that for all $t > t_0$, the following well-known bound (see, e.g., (9.9) in [14]) holds

$$(6.10) \quad \int_t^{t+\tau} \|\mathbf{u}^h(s)\|_1 ds \leq (2 + \tau\nu\lambda_1) \nu G^2.$$

We can then apply the inverse inequality (2.3) to find

$$(6.11) \quad \int_t^{t+(\nu\lambda_1)^{-1}} \|\mathbf{u}^h\|_2^2 ds \leq \tilde{C}_{2,1}^2 h^{-2} \int_t^{t+(\nu\lambda_1)^{-1}} \|\mathbf{u}^h\|_1^2 ds \leq 3\tilde{C}_{2,1}^2 h^{-2} \nu G^2.$$

Thus, if

$$(6.12) \quad \mu \geq 4C\tilde{C}_{2,1}^2 h^{-2} \nu G^2,$$

we have

$$\int_t^{t+(\nu\lambda)^{-1}} \left(\mu - \frac{C}{\nu\lambda_1} \|\mathbf{u}^h(s)\|_2^2 \right) ds \geq \frac{1}{h^2 \lambda_1} C \tilde{C}_{2,1}^2 G^2 = \gamma > 0,$$

resulting in a range

$$(6.13) \quad 4C\tilde{C}_{2,1}^2 h^{-2} \nu G^2 \leq \mu \leq \nu C_{k+1,0}^{-2} \tilde{C}_{k+1,1}^{-2} \left(\frac{h}{H} \right)^{2k} H^{-2}.$$

which, due to the factor of h^{-2} in the lower bound, is clearly not achievable.

Remark 6.3. Similar analysis can be done to show synchronization in the \mathbf{H}^1 norm, by taking $\Theta^h = \Delta \mathbf{w}^h$. In particular for $k = 1$, one can find

$$-\mu(I_H^1 \mathbf{w}^h, \Delta \mathbf{w}^h) \leq \frac{C_{1,0}^2 \tilde{C}_{3,2}^2}{2\nu} \mu \left(\frac{H}{h} \right)^2 \|\mathbf{w}^h\|_2^2 + \frac{\nu}{2} \|\mathbf{w}^h\|_2^2 - \mu \|\mathbf{w}^h\|_1^2$$

and exactly as in (3.22), (3.23) of [25]

$$\begin{aligned} |b(\mathbf{u}^h, \mathbf{u}^h, \Delta \mathbf{w}^h) - b(\mathbf{v}^h, \mathbf{v}^h, \Delta \mathbf{w}^h)| &\leq |b(\mathbf{w}^h, \mathbf{u}^h, \Delta \mathbf{w}^h)| + |b(\mathbf{v}^h, \mathbf{w}^h, \Delta \mathbf{w}^h)| \\ &\leq \frac{\nu}{4} \|\mathbf{w}^h\|_2^2 + \frac{C}{\nu} \left(1 + \frac{\|\mathbf{u}^h\|_2^2}{\lambda_1} \right) \|\mathbf{w}^h\|_1^2 \end{aligned}$$

One then can proceed as in the estimate of the L^2 error.

7. CONCLUSION

We have presented numerical simulations which demonstrate that nudging with higher order interpolation can synchronize when the data is too coarse for linear interpolation to do so, and does so faster when the data is fine enough for both to synchronize. Two flows were tested: a shear flow in an annulus, and one with a body force in a disk with an off-center obstacle, both satisfying Dirichlet

boundary conditions. We have shown rigorously that continuous data assimilation by nudging with higher order interpolation will synchronize with the solution of the spatially discretized NSE. Even without estimating the error between the nudged solution and the actual solution of the NSE, the analysis is limited in gauging the benefit of using higher order interpolation. The conditions (6.9) and (6.5) specify that a valid range for the relaxation parameter μ is

$$(7.1) \quad 2(c_0 e^{G^4} + 1) G^2 \leq \mu \leq \nu C_{k+1,0}^{-2} \tilde{C}_{k+1,1}^{-2} \left(\frac{h}{H}\right)^{2k} H^{-2}.$$

Several points are in order.

- (1) The condition (7.1) is achievable for order k interpolation, provided H , the resolution of the data, is small enough.
- (2) The higher the order k is taken, the smaller H is needed in the upper bound in (6.13). This analysis is not sensitive enough to indicate the advantage of nudging with higher order interpolation demonstrated by our numerical experiments.
- (3) The exponential factor in the Grashof number is due to assuming Dirichlet boundary conditions. A much more reasonable, algebraic in G , lower bound would suffice for periodic boundary conditions. Though in either case the restriction may seem impractical for turbulent flows that require large G , our simulations suggest it is far from sharp, as has been shown to be the case in comparing other numerical tests of nudging with corresponding analyses [11, 19, 31, 34].

REFERENCES

- [1] M. U. Altaf, E. S. Titi, T. Gebrael, O. M. Knio, L. Zhao, M. F. McCabe, and I. Hoteit, *Downscaling the 2D Bénard convection equations using continuous data assimilation*, Comput. Geosci. **21** (2017), no. 3, 393–410.
- [2] M. Asch, M. Bocquet, and M. Nodet, *Data assimilation*, Fundamentals of Algorithms, vol. 11, Society for Industrial and Applied Mathematics (SIAM), Philadelphia, PA, 2016. Methods, algorithms, and applications.
- [3] D. Auroux and J. Blum, *A nudging-based data assimilation method: the Back and Forth Nudging (BFN) algorithm*, Nonlin. Processes Geophys. **15** (2008), 305–319.
- [4] A. Azouani, E. Olson, and E. S. Titi, *Continuous data assimilation using general interpolant observables*, J. Nonlinear Sci. **24** (2014), no. 2, 277–304.
- [5] H. Bessaih, E. Olson, and E. S. Titi, *Continuous data assimilation with stochastically noisy data*, Nonlinearity **28** (2015), no. 3, 729–753.
- [6] A. Biswas, K. Brown, and V. Martinez, *Higher-order synchronization for a data assimilation algorithm with nodal value observables for the Navier-Stokes equation*, preprint (2021).
- [7] A. Biswas, C. Foias, C. F. Mondaini, and E. S. Titi, *Downscaling data assimilation algorithm with applications to statistical solutions of the Navier-Stokes equations*, Ann. Inst. H. Poincaré Anal. Non Linéaire **36** (2019), no. 2, 295–326.
- [8] A. Biswas, J. Hudson, A. Larios, and Y. Pei, *Continuous data assimilation for the 2D magnetohydrodynamic equations using one component of the velocity and magnetic fields*, Asymptot. Anal. **108** (2018), no. 1-2, 1–43.
- [9] A. Biswas, M. Jolly, and Z. Bradshaw, *Data assimilation for the Navier-Stokes equations using local observables*, SIAM J. Appl. Dyn. Sys. **(to appear)** (2021).
- [10] S. C. Brenner and L. R. Scott, *The mathematical theory of finite element methods*, Third, Texts in Applied Mathematics, vol. 15, Springer, New York, 2008.

- [11] Y. Cao, M. S. Jolly, E. S. Titi, and J. P. Whitehead, *Algebraic bounds on the Rayleigh-Bénard attractor*, Nonlinearity **34** (2021), no. 1, 509–531.
- [12] J. Charney, M. Halem, and R. Jastrow, *Use of incomplete historical data to infer the present state of the atmosphere*, J. Atmos. Sci. **26** (1969), 1160–1163.
- [13] B. Cockburn, D. A. Jones, and E. S. Titi, *Estimating the number of asymptotic degrees of freedom for nonlinear dissipative systems*, Math. Comp. **66** (1997), no. 219, 1073–1087.
- [14] P. Constantin and C. Foias, *Navier-Stokes equations*, Chicago Lectures in Mathematics, University of Chicago Press, Chicago, IL, 1988.
- [15] P. Constantin, C. Foias, O. P. Manley, and R. Temam, *Determining modes and fractal dimension of turbulent flows*, J. Fluid Mech. **150** (1985), 427–440.
- [16] J. A. De Loera, J. Rambau, and F. Santos, *Triangulations*, Algorithms and Computation in Mathematics, vol. 25, Springer-Verlag, Berlin, 2010. Structures for algorithms and applications.
- [17] G. Evensen, *Data assimilation*, Second, Springer-Verlag, Berlin, 2009. The ensemble Kalman filter.
- [18] A. Farhat, N. E. Glatt-Holtz, V. R. Martinez, S. A. McQuarrie, and J. P. Whitehead, *Data assimilation in large Prandtl Rayleigh-Bénard convection from thermal measurements*, SIAM J. Appl. Dyn. Syst. **19** (2020), no. 1, 510–540.
- [19] A. Farhat, H. Johnston, M. Jolly, and E. S. Titi, *Assimilation of nearly turbulent Rayleigh-Bénard flow through vorticity or local circulation measurements: a computational study*, J. Sci. Comput. **77** (2018), no. 3, 1519–1533.
- [20] A. Farhat, M. Jolly, and E. S. Titi, *Continuous data assimilation for the 2D Bénard convection through velocity measurements alone*, Phys. D **303** (2015), 59–66.
- [21] A. Farhat, E. Lunasin, and E. S. Titi, *A data assimilation algorithm: the paradigm of the 3D Leray- α model of turbulence*, Partial differential equations arising from physics and geometry, London Math. Soc. Lecture Note Ser., vol. 450, Cambridge Univ. Press, Cambridge, 2019, pp. 253–273.
- [22] ———, *Continuous data assimilation for a 2D Bénard convection system through horizontal velocity measurements alone*, J. Nonlinear Sci. **27** (2017), no. 3, 1065–1087.
- [23] ———, *Data assimilation algorithm for 3D Bénard convection in porous media employing only temperature measurements*, J. Math. Anal. Appl. **438** (2016), no. 1, 492–506.
- [24] ———, *Abridged continuous data assimilation for the 2D Navier-Stokes equations utilizing measurements of only one component of the velocity field*, J. Math. Fluid Mech. **18** (2016), no. 1, 1–23.
- [25] A. Farhat, M. Jolly, and E. S. Titi, *Continuous data assimilation for the 2D Bénard convection through velocity measurements alone*, Phys. D **303** (2015), 59–66.
- [26] A. Farhat, E. Lunasin, and E. S. Titi, *Abridged continuous data assimilation for the 2D Navier-Stokes equations utilizing measurements of only one component of the velocity field*, J. Math. Fluid Mech. **18** (2016), no. 1, 1–23.
- [27] U. Frisch, *Turbulence*, Cambridge University Press, Cambridge, 1995. The legacy of A. N. Kolmogorov.
- [28] C. Foias, C. F. Mondaini, and E. S. Titi, *A discrete data assimilation scheme for the solutions of the two-dimensional Navier-Stokes equations and their statistics*, SIAM J. Appl. Dyn. Syst. **15** (2016), no. 4, 2109–2142.
- [29] C. Foias and G. Prodi, *Sur le comportement global des solutions non-stationnaires des équations de Navier-Stokes en dimension 2*, Rend. Sem. Mat. Univ. Padova **39** (1967), 1–34.
- [30] B. García-Archilla, J. Novo, and E. S. Titi, *Uniform in time error estimates for a finite element method applied to a downscaling data assimilation algorithm for the Navier-Stokes equations*, SIAM J. Numer. Anal. **58** (2020), no. 1, 410–429.
- [31] M. Gesho, E. Olson, and E. S. Titi, *A computational study of a data assimilation algorithm for the two-dimensional Navier-Stokes equations*, Commun. Comput. Phys. **19** (2016), no. 4, 1094–1110.
- [32] M. D. Gunzburger, *Finite element methods for viscous incompressible flows*, Computer Science and Scientific Computing, Academic Press, Inc., Boston, MA, 1989. A guide to theory, practice, and algorithms.
- [33] W. D. Henshaw, H. Kreiss, and J. Yström, *Numerical experiments on the interaction between the large- and small-scale motions of the Navier-Stokes equations*, Multiscale Model. Simul. **1** (2003), no. 1, 119–149.

- [34] J. Hudson and M. Jolly, *Numerical efficacy study of data assimilation for the 2D magnetohydrodynamic equations*, J. Comput. Dyn. **6** (2019), no. 1, 131–145.
- [35] F. Hecht, *New development in FreeFem++*, J. Numer. Math. **20** (2012), no. 3-4, 251–265.
- [36] J. E. Hoke and R. A. Anthes, *The initialization of numerical models by a dynamic initialization technique*, Monthly Weather Review **104** (1976), 1551–1556.
- [37] H. A. Ibdah, C. F. Mondaini, and E. S. Titi, *Fully discrete numerical schemes of a data assimilation algorithm: uniform-in-time error estimates*, IMA J. Numer. Anal. **40** (2020), no. 4, 2584–2625.
- [38] N. Jiang and W. Layton, *An algorithm for fast calculation of flow ensembles*, Int. J. Uncertain. Quantif. **4** (2014), no. 4, 273–301.
- [39] M. S. Jolly, V. R. Martinez, E. J. Olson, and E. S. Titi, *Continuous data assimilation with blurred-in-time measurements of the surface quasi-geostrophic equation*, Chin. Ann. Math. Ser. B **40** (2019), no. 5, 721–764.
- [40] M. Jolly, T. Sadigov, and E. S. Titi, *Determining form and data assimilation algorithm for weakly damped and driven Korteweg–de Vries equation—Fourier modes case*, Nonlinear Anal. Real World Appl. **36** (2017), 287–317.
- [41] M. Jolly, V. R. Martinez, and E. S. Titi, *A data assimilation algorithm for the subcritical surface quasi-geostrophic equation*, Adv. Nonlinear Stud. **17** (2017), no. 1, 167–192.
- [42] V. John, *Finite element methods for incompressible flow problems*, Springer Series in Computational Mathematics, vol. 51, Springer, Cham, 2016.
- [43] D. A. Jones and E. S. Titi, *Determining finite volume elements for the 2D Navier-Stokes equations*, Phys. D **60** (1992), no. 1-4, 165–174. Experimental mathematics: computational issues in nonlinear science (Los Alamos, NM, 1991).
- [44] D. A. Jones and E. S. Titi, *Upper bounds on the number of determining modes, nodes, and volume elements for the Navier-Stokes equations*, Indiana Univ. Math. J. **42** (1993), no. 3, 875–887.
- [45] A. Larios, L. Rebholz, and C. Zervas, *Global in time stability and accuracy of IMEX-FEM data assimilation schemes for Navier-Stokes equations*, Comput. Methods Appl. Mech. Engrg. **345** (2019), 1077–1093.
- [46] W. Layton, *Introduction to the numerical analysis of incompressible viscous flows*, Computational Science & Engineering, vol. 6, Society for Industrial and Applied Mathematics (SIAM), Philadelphia, PA, 2008.
- [47] K. Law, A. Stuart, and K. Zygalakis, *Data assimilation*, Texts in Applied Mathematics, vol. 62, Springer, Cham, 2015. A mathematical introduction.
- [48] C. F. Mondaini and E. S. Titi, *Uniform-in-time error estimates for the postprocessing Galerkin method applied to a data assimilation algorithm*, SIAM J. Numer. Anal. **56** (2018), no. 1, 78–110.
- [49] E. Kalnay, *Atmospheric modeling, data assimilation, and predictability*, Cambridge Univ Pr, 2003.
- [50] P. A. Markowich, E. S. Titi, and S. Trabelsi, *Continuous data assimilation for the three-dimensional Brinkman–Forchheimer-extended Darcy model*, Nonlinearity **29** (2016), no. 4, 1292–1328.
- [51] S. Pawar, S. E. Ahmed, O. San, A. Rasheed, and I. M. Navon, *Long short-term memory embedded nudging schemes for nonlinear data assimilation of geophysical flows*, Physics of Fluids **32** (2020).
- [52] L. M. Pecora and T. L. Carroll, *Synchronization of chaotic systems*, Chaos **25** (2015), no. 9, 097611, 12.
- [53] Y. Pei, *Continuous data assimilation for the 3D primitive equations of the ocean*, Commun. Pure Appl. Anal. **18** (2019), no. 2, 643–661.
- [54] C. Taylor and P. Hood, *A numerical solution of the Navier-Stokes equations using the finite element technique*, Internat. J. Comput. & Fluids **1** (1973), no. 1, 73–100.
- [55] P. A. Vidard, F.-X. Le Dimet, and A. Piacentini, *Determination of optimal nudging coefficients*, Tellus A: Dynamic Meteorology and Oceanography **55** (2003), no. 1, 1–15.
- [56] C. Zervas, L. G. Rebholz, M. Schneier, and T. Iliescu, *Continuous data assimilation reduced order models of fluid flow*, Comput. Methods Appl. Mech. Engrg. **357** (2019), 112596, 18.